

# **Solvent determines nature of effective interactions between nanoparticles in polymer brushes**

Zengju Lian,<sup>\*,†</sup> Shuanhu Qi,<sup>‡</sup> Jiajia Zhou,<sup>‡</sup> and Friederike Schmid<sup>‡</sup>

*Department of Physics, Ningbo University, Ningbo 315200, P. R. China, and Institut für Physik,  
Johannes Gutenberg-Universität Mainz, D55099 Mainz, Germany*

E-mail: lzju98@gmail.com/lianzengju@nbu.edu.cn

---

\*To whom correspondence should be addressed

†Department of Physics, Ningbo University, Ningbo 315200, P. R. China

‡Institut für Physik, Johannes Gutenberg-Universität Mainz, D55099 Mainz, Germany

## Abstract

We study the effective interaction between two parallel rod-like nanoparticles in swollen and collapsed polymer brushes as a function of penetration depth by two-dimensional self-consistent field calculations. In vertical direction, the interaction is always attractive. In lateral direction, the behavior in good and poor solvent conditions is qualitatively different. In swollen brushes (good solvent), nanoparticles always repel each other. In collapsed brushes (poor solvent), we identify two different regimes: An immersed regime where the nanoparticles are fully surrounded by the brush, and an interfacial regime, where they are located in the interface between brush and solvent. In the immersed regime, the lateral interactions are repulsive, in agreement with previous theoretical predictions. In the interfacial regime, they are governed by the deformations of the interface and tend to be attractive. This implies that the nature of nanoparticle interactions can be manipulated by changing the solvent condition. The influence of particle size and grafting density are also briefly discussed.

## 1 Introduction

Nanoparticle dispersions have been studied intensively for a long time because they are interesting model systems for fundamental research and because they can be used to engineer novel materials.<sup>1,2</sup> By blending nanoparticles, e.g., with polymers, one may obtain an end product that combines the properties and functionalities of its constituents. To optimize such materials, one must understand the organization and the distribution of nanoparticles. The first step in this direction is to study the effective interactions between pairs of particles, because they determine the particle assembly at low particle density. At higher densities, multi-body potentials may become important; however a model based on effective pair interactions can still serve as a good starting point for the development of more sophisticated theories. One prominent example of such a model is the Asakura-Oosawa model,<sup>3-5</sup> which describes the effective pair interactions between colloids in dilute polymer solution. If two nanoparticles approach each other, polymer molecules are driven out of the space between the nanoparticles, and this creates an effective depletion interaction between

colloidal particles. A related depletion effect is also found in dense polymer solutions.<sup>6</sup>

The situation is more complicated when polymers are grafted to a surface (polymer brush). In this case, polymers cannot move away as a whole. This changes the nature of interactions. Nanoparticle-brush mixtures are interesting for several reasons: Firstly, they can serve as model systems to investigate important nanoscale processes in biological environments.<sup>7-12</sup> In biology, many vital activities related to intercellular transport and communication depend on the interactions of nanoscaled objects – such as protein complexes and viruses – with biopolymer-covered surfaces – such as blood capillaries or cell membranes. Physical aspects of these systems can be mimicked by systems containing nanoparticles and polymer brushes. The study of nanoparticle-brush mixtures can also give insights into the physical basis of selectivity in biological processes such as protein adsorption or the immune response.<sup>13-16</sup> Secondly, an improved understanding of nanoparticle organization in polymer brushes can help to design novel nanostructured materials in nanotechnology.<sup>17-22</sup> Surface grafting of polymer chains is an increasingly popular method to modify the properties of surfaces. Grafted polymers can be used to assist the assembly of nanostructured materials exposed to a nanoparticle suspension.<sup>17,18,21</sup> A better understanding of the effective interaction between the nanoparticles can help to optimize the process of self-assembly and to develop design principles for new materials.

The theoretical interest in polymer brush-nanoparticle systems goes back to a seminal paper by Williams and Pincus,<sup>23</sup> who calculated the forces acting on small fillers in a polymer brush of infinite thickness by establishing an analogy with hydrodynamics. Subramaniam *et al.* and Steels *et al.* analyzed the deformation of single grafted polymer and polymer brushes due to compression by particles of finite size.<sup>24,25</sup> Other authors addressed the question how to prevent the adsorption of nanoparticles or proteins onto surfaces as a function of particle size, grafting density, surface chemistry, and chain length, for applications in the context of nanoparticle stabilization, the fabrication of anti-fouling surfaces and biomedicine.<sup>26-30</sup> While most studies focused on the interactions of individual particles with brushes, some also considered the polymer-mediated interactions between nanoparticles. Using a perturbative approach, Solis and Tang investigated the

interactions between two point-like density perturbations in a collapsed melt-like brush.<sup>31,32</sup> They predicted that the interaction is mainly repulsive, with possibly a weakly oscillatory component at distances larger than the brush height. Chen and Ma<sup>33</sup> studied the special case where a dry polymer brush is in contact with a polymer melt by self-consistent field calculations. They found that the effective interaction is repulsive at large distances, possibly supplemented by a short range attractive contribution. Curk *et al.*<sup>18,34</sup> used Monte Carlo simulations to investigate the collective ordering of nanoparticles in a polymer brush. When large amounts of nanoparticles are pressed into a swollen brush by external forces, they are found to form columnar structures perpendicular to the brush surface and to microphase separate in the lateral directions. The structures of droplets of polymer-insoluble nanoparticles in brushes were also studied by theory<sup>28</sup> and dissipative particle dynamics simulations.<sup>35,36</sup>

With respect to applications in biotechnology<sup>37–39</sup> and the fabrication of nanomaterials,<sup>17,40</sup> the effect of the solvent condition on nanoparticle-brush mixtures is of particular interest. For example, processing in nanotechnology often involves a step where one solvent is replaced by another, therefore it is important to understand how this may affect the interactions in the system. The influence of solvent quality on the structure of pure brushes has been known for a long time:<sup>30,41–43</sup> Polymer brushes collapse in poor solvent but swell in good solvent. One would expect that the difference in the chain conformations results in different behavior of the immersed nanoparticles. This could provide an opportunity to control the structure of the multi-particle assembly by using stimuli-responsive polymers, which can alter their properties in response to the environmental changes.<sup>44,45</sup> Therefore, it is important to understand the nanoparticle-brush system under different solvent conditions.

The influence of the solvent quality on the nanoparticle uptake in polymer brushes has recently been studied theoretically by Halperin *et al.*<sup>30</sup> They predict that particles can only penetrate a brush if their size does not exceed a solvent-dependent “insertion length” which decreases with increasing solvent quality. Hence penetration is facilitated when the solvent is poorer. The aggregation behavior of nanoparticles should also depends on the solvent. However, to our best knowledge, the

influence of solvent quality on the nanoparticle pair interactions in a brush has not yet been studied systematically.

Motivated by the above observations, in the present paper, we study the effective interactions of rod-like nanoparticles immersed in polymer brushes under different solvent conditions. We utilize the self-consistent field theory, which is a powerful method for studying the phase behavior of polymer systems.<sup>46–48</sup> In a nutshell, our results can be summarized as follows: The effective interactions in lateral direction (parallel to the substrate) depend on solvent quality and on the penetration depth of particles. In good solvent, nanoparticles always repel each other. In poor solvent, they repel each other when they are deeply immersed in the brush, but they attract each other when they approach the brush surface. In contrast, the effective interactions in transverse direction (perpendicular to the substrate) are always attractive, independent of solvent quality. We identify the main factors governing the transition between the attractive and the repulsive regime by analyzing the different entropic and energetic contributions to the interaction energy, as well as the influence of particle size and grafting density.

The rest of our paper is organized as follows: We introduce the framework of the self-consistent field theory and describe our model parameters in Section Section 2. We then present our main results on the effective interaction in Section Section 3, and analyze the effects of the penetration depth, the particle size and the grafting density of the brush for both good and poor solvent. Our results are discussed and summarized in Section Section 4.

## 2 Model and Theory

We consider an incompressible system of two parallel rod-like nanoparticles immersed in a solvent-polymer mixture with volume  $V$ . All  $n_p$  polymer chains are grafted on a flat substrate, and they have the same polymerization index  $N$  with the same statistical segment length  $b$ . The solvent quality is described by the Flory-Huggins parameter  $\chi$ , which is related to the excluded volume per segment  $v$  as  $v = 1 - 2\chi$  scaled by the segment volume. Good solvent corresponds to  $\chi < 0.5$ ,

while poor solvent corresponds to the range  $\chi > 0.5$ . The dividing point  $\chi = 0.5$  defines the  $\Theta$  solvent in which the excluded volume parameter vanishes. In good solvent, the solvent fills almost the whole system, whereas in poor solvent, it is almost entirely driven out of the brush due to the repulsion between solvent and polymer. For simplicity, we assume that solvent molecules and polymer segments have the same volume, given by  $\rho^{-1}$ . The effect of the solvent size has been discussed in Ref.<sup>49</sup> Solvents and polymer segments cannot penetrate the nanoparticle. In the literature, different ways have been proposed to implement this impenetrability condition. One method is to introduce a steeply repulsive monomer-particle potential around the particle,<sup>50,51</sup> the other is to represent the particle by a ‘‘cavity function’’ that assigns a local volume fraction of value unity to a nanoparticle in an extended region of space.<sup>33,52–54</sup> In the present work, we adopt the cavity function method. The nanoparticle is modeled by infinitely elongated cylinder of radius  $R$  surrounded by a boundary layer of thickness  $\Delta$ , and we set  $\Delta = 2b$ . The boundary layer mimicks the effect of surface roughness and/or soft organic coatings on the nanoparticle. We describe it in terms of a cosine function as in Refs.<sup>33,55</sup> The local volume fraction of a nanoparticle  $\psi_c(\mathbf{r})$  with center at position  $\mathbf{r}_c$  is thus described by a function of the form

$$\psi_c(\mathbf{r}) = \begin{cases} 1 & |\mathbf{r} - \mathbf{r}_c| \leq R \\ [1 + \cos((|\mathbf{r} - \mathbf{r}_c| - R)\pi/\Delta)]/2 & R \leq |\mathbf{r} - \mathbf{r}_c| \leq R + \Delta \\ 0 & |\mathbf{r} - \mathbf{r}_c| \geq R + \Delta \end{cases} \quad (1)$$

The positions of the particles are kept fixed in every calculation. They are characterized by three parameters: The distance between the first particle and the substrate,  $h$ , the lateral distance between the particles,  $d$ , and the angle between the vector connecting the particle centers and its projection on the substrate,  $\theta$  (with  $0 \leq \theta \leq \pi/2$ ) (see Fig. Figure 1).

Since we impose an incompressibility constraint, nanoparticles cannot come closer than the center-center distance ( $2R + \Delta$ ) (otherwise the total nanoparticle volume fraction would exceed one in the contact region). As long as this condition is met, the numbers of the solvents and the polymer chains in the system do not depend on the nanoparticle positions. Therefore, the free

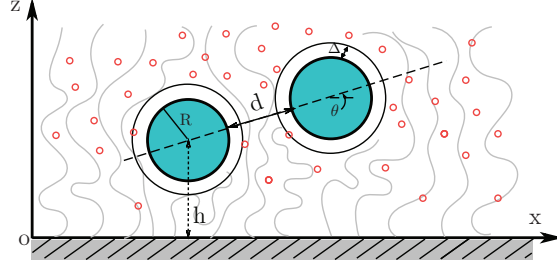


Fig. 1: Schematic view of two nanoparticles immersed in a solvent-brush mixture. Note that the boundary layers of thickness  $\Delta$  may overlap.

energy of the system can be calculated in the canonical ensemble for fixed  $V$  and temperature  $T$ . The free energy of the system has two contributions. One is the interaction energy of the solvents, the polymer chains and the nanoparticles,  $U$ , the other includes entropy contributions of the solvents  $S_s$  and the polymer chains  $S_p$ . The total free energy has the form  $F_t = U - (S_s + S_p)T$ . Within the mean-field approximation to the many-chains Edwards theory,<sup>46,56–58</sup> the interaction energy and the entropies of the polymers and the solvents at a temperature  $T$  can be expressed as follows

$$\frac{NU}{\rho k_B T V} = \frac{N}{V} \int d\mathbf{r} [\chi_{pc} \psi_p(\mathbf{r}) \psi_c(\mathbf{r}) + \chi_{ps} \psi_s(\mathbf{r}) \psi_p(\mathbf{r}) + \chi_{cs} \psi_s(\mathbf{r}) \psi_c(\mathbf{r})] \quad (2)$$

$$\frac{NS_p}{\rho k_B V} = \bar{\psi}_p \ln \frac{Q_p}{\bar{\psi}_p V} + \frac{1}{V} \int d\mathbf{r} w_p(\mathbf{r}) \psi_p(\mathbf{r}) \quad (3)$$

$$\frac{NS_s}{\rho k_B V} = \bar{\psi}_s N \ln \frac{Q_s}{\bar{\psi}_s V} + \frac{1}{V} \int d\mathbf{r} w_s(\mathbf{r}) \psi_s(\mathbf{r}) \quad (4)$$

with the Boltzmann constant  $k_B$ . The spatial integration is restricted to a rectangular box with the volume  $V = L_x \times L_z$ . Here,  $L_x$  and  $L_z$  are chosen large enough to avoid finite size effects.  $\chi_{ps}$ ,  $\chi_{pc}$  and  $\chi_{cs}$  are Flory-Huggins interaction parameters characterizing the polymer-solvent, the polymer-nanoparticle and the solvent-nanoparticle interactions, respectively.  $\psi_s(\mathbf{r})$  and  $\psi_p(\mathbf{r})$  are the local fractions of the solvents and the polymer chains, while  $\bar{\psi}_s$  and  $\bar{\psi}_p$  express their overall volume fractions.  $w_p(\mathbf{r})$  and  $w_s(\mathbf{r})$  are the conjugate fields to  $\psi_s(\mathbf{r})$  and  $\psi_p(\mathbf{r})$ , respectively, and  $Q_p = \int \mathcal{D}\mathbf{R} \exp[-\mathcal{H}^0[\mathbf{R}] - \int_0^1 ds w_p(\mathbf{R}(s))]$  is the partition function for a single polymer in the mean

fields  $w_p$ . Here,  $\mathcal{H}^0[\mathbf{R}] = \frac{3N}{2b^2} \int_0^1 ds \left( \frac{d\mathbf{R}(s)}{ds} \right)^2$  is defined as the elastic free energy of the polymer chain and  $\mathbf{R}(s)$  is the position of segment  $s$  on the polymer chain.  $Q_s = \int d\mathbf{r} \exp[-w_s(\mathbf{r})/N]$  denotes the partition function of the solvent.

Minimizing the free energy with respect to the local volume fractions and their conjugate fields leads to a set of mean-field equations

$$w_p = N\chi_{ps}(\psi_s - \psi_p) + N(\chi_{pc} - \chi_{cs})\psi_c - N \ln \psi_s \quad (5)$$

$$\psi_p = \frac{\bar{\psi}_p V}{Q_p} \int_0^1 ds q(\mathbf{r}, s) q^\dagger(\mathbf{r}, 1-s) \quad (6)$$

$$w_s = -N \ln \psi_s \quad (7)$$

$$\psi_s = 1 - \psi_p - \psi_c. \quad (8)$$

with  $Q_p = \int d\mathbf{r} q(\mathbf{r}, 1)$ . The last equation is the incompressibility constraint, which we enforce rigorously instead of introducing an auxiliary pressure field as is often done in related self-consistent field approaches to polymer systems.<sup>46</sup> Here we have shifted the local field  $w_s(r)$  by a constant  $w_0$  for numerical convenience, choosing  $w_0$  such that  $Q_s/\bar{\psi}_s V = 1$ . Shifting  $w_s$  does not change the value of the free energy, but the expression for  $F_t$  becomes simpler:

$$\begin{aligned} \frac{NF_t}{\rho_0 k_B T V} = & -\bar{\psi}_p \ln \frac{Q_p}{\bar{\psi}_p V} + \frac{1}{V} \int d\mathbf{r} [\chi_{pc} N \psi_p(\mathbf{r}) \psi_c(\mathbf{r}) + \chi_{ps} N \psi_s(\mathbf{r}) \psi_p(\mathbf{r}) \\ & + \chi_{cs} N \psi_s(\mathbf{r}) \psi_c(\mathbf{r}) + N \psi_s(\mathbf{r}) \ln \psi_s(\mathbf{r}) - w_p(\mathbf{r}) \psi_p(\mathbf{r})] \end{aligned} \quad (9)$$

The partial partition function  $q^\dagger(\mathbf{r}, s) = \int \mathcal{D}\mathbf{R} \exp[-\mathcal{H}_s^0[\mathbf{R}] - \int_0^s ds' w_p(\mathbf{R}(s'))] \cdot \delta(\mathbf{R}(s) - \mathbf{r})$  in Eq. (Figure 1) (with  $\mathcal{H}_s^0[\mathbf{R}] = \frac{3N}{2b^2} \int_0^s ds' \left( \frac{d\mathbf{R}(s')}{ds'} \right)^2$ ) describes a chain propagator from the free end of the chain to the  $s$ th segment at position  $\mathbf{r}$  and satisfies a modified diffusion equation

$$\frac{\partial q^\dagger(\mathbf{r}, s)}{\partial s} = \frac{Nb^2}{6} \nabla^2 q^\dagger(\mathbf{r}, s) - w_p(\mathbf{r}) q^\dagger(\mathbf{r}, s) \quad (10)$$

with the initial conditions  $q^\dagger(\mathbf{r}, s=0) = \delta(z)$ . The function  $q(\mathbf{r}, s)$  is the analogous function that describes the chain propagator from the grafted end with an initial condition  $q(\mathbf{r}, s=0) = \delta(z)$ .

Note that this formalism describes brushes of laterally mobile chains, i.e., grafting points can move along the substrate. At high grafting densities, the behavior of brushes with mobile and immobile grafting points is very similar.

Having obtained the total free energy of the system, one can calculate the effective pair interaction energy of two nanoparticles,  $F$ , from

$$F = F_t - F_1^P - F_2^P + F_0, \quad (11)$$

where,  $F_i^P$  is the free energy of the solvent-brush system with a single nanoparticle immersed in the brush at the same position as the nanoparticle  $i$  in the total system, and  $F_0$  is the free energy of the same solvent-brush system without nanoparticles. The contributions of the interaction energy and the entropies of polymers and solvent to the effective pair interaction are calculated in a similar manner.

Before proceeding to the presentation of the numerical results, we first briefly discuss the behavior of a system containing two nanoparticles immersed in pure solvent. Due to the incompressibility of the system, according the equation (Figure 1), the solvent entropy can be written as

$$\frac{NS_s^0}{\rho k_B V} = \frac{N}{V} \int d\mathbf{r} (\psi_c(\mathbf{r}) - 1) \ln(1 - \psi_c(\mathbf{r})) = \frac{N}{V} \int d\mathbf{r} f_s(\mathbf{r}) \quad (12)$$

where  $f_s(\mathbf{r}) \equiv (-\psi_c(\mathbf{r}) - 1) \ln(1 - \psi_c(\mathbf{r}))$ . In addition, in pure solvent, the interaction energy  $U$  assumes the simple form

$$\frac{NU^0}{\rho k_B T V} = \frac{N}{V} \chi_{cs} \left[ \int d\mathbf{r} \psi_c(\mathbf{r})(1 - \psi_c(\mathbf{r})) \right] = \frac{N}{V} \chi_{cs} \int d\mathbf{r} f_u(\mathbf{r}). \quad (13)$$

with  $f_u(\mathbf{r}) \equiv \psi_c(\mathbf{r})(1 - \psi_c(\mathbf{r}))$ . Obviously,  $S_s^0$  and  $U^0$  change only when the boundary layers of the particles overlap, and one can easily check that both  $S_s^0$  and  $U^0$  decrease with decreasing particle distance  $d$ . Due to the competition of the solvent entropy and the interaction energy of the system, the nanoparticles attract each other when  $\Delta U^0 > \Delta S_s^0 T$ , while they repel each other when

$\Delta U^0 < \Delta S_s^0$ . Here,  $\Delta U^0$  and  $\Delta S_s^0$  indicate the change of  $U^0$  and  $S_s^0$ , respectively, as the particles approach each other. The result of the competition of these two contributions in solvent is mainly determined by  $\chi_{cs}$ . In the following, we set  $\chi_{cs} = 0.2$ , a value where the interaction between the particles in pure solvent is weakly repulsive.

### 3 Results and discussion

In the present paper, we solve the self-consistent mean field equations within a two-dimensional Cartesian framework (grid size  $0.125b$  in both directions) with periodical boundary conditions in the  $x$ -direction, Dirichlet boundary conditions at  $z = 0$ , and Neumann boundary conditions at  $z = L_z$ . The modified diffusion equation is solved in real-space using the Crank-Nicolson method combined with the Alternating Direction Implicit method. The self-consistent equations are solved by iteration using simple mixing<sup>48</sup>. All lengths are scaled by the segment size  $b$ . The polymerization of the polymer chain is  $N = 100$ . We compare systems with  $\chi_{ps} = 0$  and  $\chi_{ps} = 1$ , corresponding to a good and a poor solvent, respectively. For simplicity,  $\chi_{pc}$  and  $\chi_{cs}$  are set to the same value,  $\chi_{pc} = \chi_{cs} = 0.2$ . The particle size  $R$  is varied from  $R = 0.5R_g$  to  $R = 1.75R_g$  with  $R_g = \sqrt{N/6} = 4.08$ , and the grafting density from  $\sigma = 0.09$  to  $\sigma = 0.22$ .

#### 3.1 Effective interactions in lateral direction

We first consider the situation where both particles are arranged at the same distance  $h$  from the substrate ( $\theta = 0$  in Fig. Figure 1). Fig. Figure 2 (top) shows the effective lateral pair interactions  $F$  between two particles with radius  $R = 1.25R_g = 5.1$  in brushes with grafting density  $\sigma = 0.16$  under good and poor solvent conditions. The lower panels illustrate the contributions from the “solvent free energy”  $U - TS_s$ , the interaction energy  $U$ , and the polymer entropy  $S_p$ . (We recall that the effective pair interaction is given by  $F = U - T(S_s + S_p)$ ). We only consider particle separations  $d > 2\Delta$ , where the boundary layers don’t overlap and the nanoparticles don’t interact directly with each other, hence the effective interactions are entirely mediated by the surrounding

solvent and/or polymer. As explained in Sec. Section 2, all quantities,  $F, U, S_s$ , and  $S_p$ , are shifted such that they vanish at infinite particle distance.

Under good solvent conditions (left panels in Fig. Figure 2), the pair interaction is purely repulsive, and decreases continuously with increasing distance from the substrate  $h$ . It is dominated by the solvent free energy, which also decays monotonically with increasing  $d$  and  $h$ . Since the energetic contribution  $U$  vanishes at  $\chi_{ps} = 0$ , the solvent free energy is essentially given by the solvent entropy. The behavior of the polymer entropy is more interesting: As the nanoparticles approach each other, coming from large separation  $d$ , the polymer entropy first rises to a *positive* value, i.e., the polymers *gain* entropy. The reason is that polymers in good solvent are swollen. If they are slightly compressed, the internal stretching of polymers is reduced and they gain entropy (this is, of course, more than compensated by the corresponding loss of solvent entropy). If they are strongly compressed, they lose entropy. The polymer material underneath the nanoparticles is slightly compressed, but it can escape sideways. When the nanoparticles approach each other, escaping becomes more difficult, and the total amount of slightly compressed polymer material increases, i.e., the entropy  $S_p$  increases. At smaller  $d$  and small particle-substrate distances  $h$ , this trend reverses, and  $S_p$  may become negative. Here, an additional effect comes into play: The polymer density in the gap between the particles increases (see Fig. Figure 3(a)), indicating that the material in the gap becomes more strongly compressed. This can be explained within the classical scaling theory for polymers,<sup>59</sup> which predicts that the monomer density in solutions of swollen polymers increases under confinement. The corresponding contribution to  $S_p$  is negative, and as a result, the behavior of  $S_p$  may become nonmonotonic and exhibit a maximum as a function of the particle separation  $d$ . The total pair free energy, however, is still a monotonously decaying function of  $d$  as explained above.

In poor solvent, the situation is more complicated (Fig. Figure 2, right panels). At small particle-substrate distance  $h < 16$ , the pair interaction is repulsive like in the swollen brush. At larger  $h$ , however, it becomes attractive. We will now analyze this finding in more detail. First, we note that the collapsed brush layer is of course thinner than the swollen brush layer. Fig. Figure 4

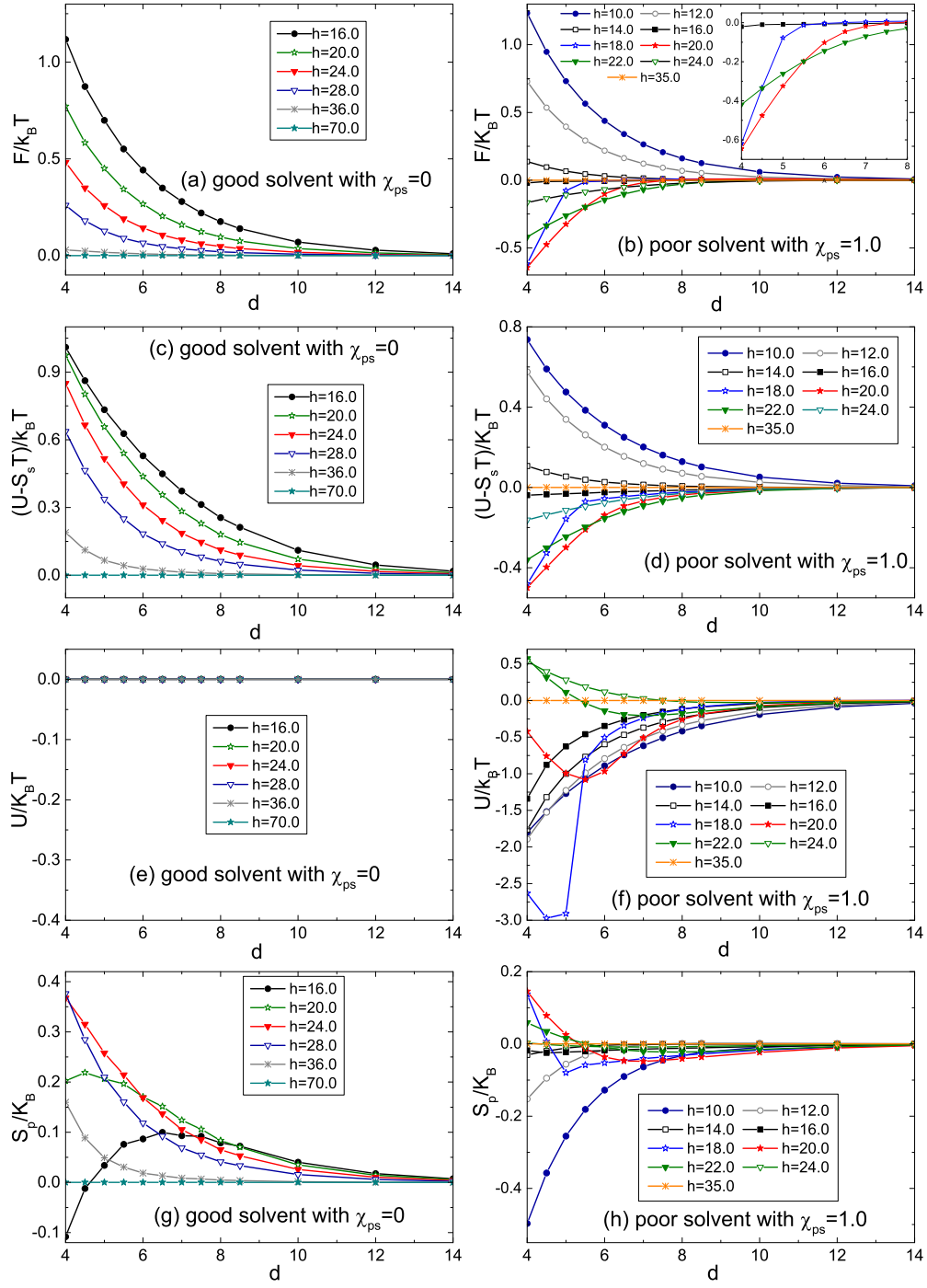


Fig. 2: Effective pair interactions  $F/k_B T$  (a,b), “solvent free energies”  $(U - S_s T)/k_B T$  (c,d), interaction energies  $U/k_B T$  (e,f), and polymer entropies  $S_p/k_B$  (g,h) in lateral direction between two nanoparticles with surface-to-surface separation  $d$  in a polymer brush for different distances  $h$  from the substrate as indicated. Left graphs correspond to good solvent conditions with  $\chi_{ps} = 0$ , right graphs to poor solvent conditions with  $\chi_{ps} = 1$ . Inset in (b) shows detail for  $h = 16, 18, 20$ , and  $22$ . The particle size is  $R = 1.25R_g = 5.1$  and the grafting density is  $\sigma = 0.16$ .

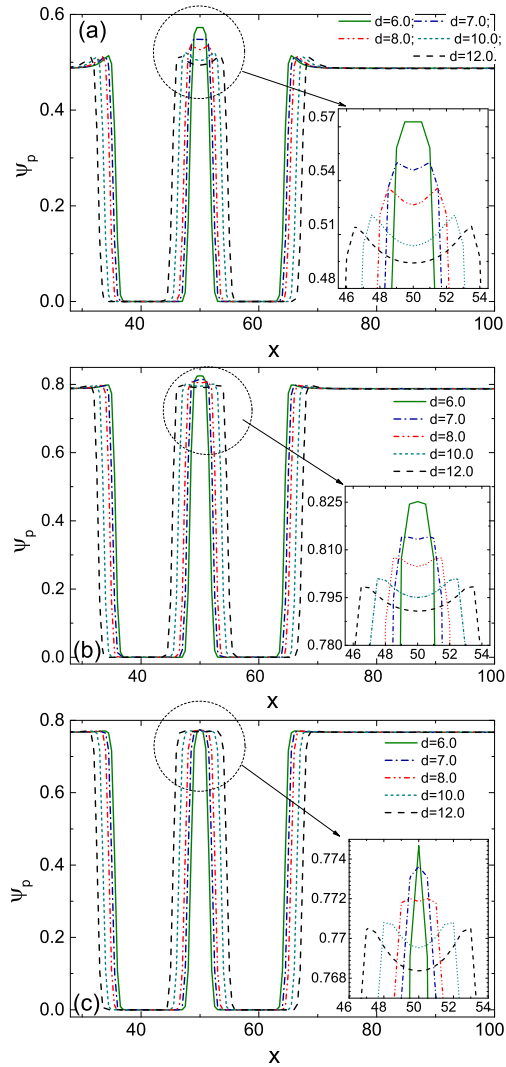


Fig. 3: Profiles of polymer volume fraction in  $x$ -direction at  $z = h$  for good solvent (a) and poor solvent (b,c) for nanoparticles with distance from the substrate  $h = 16$  (a,c) and  $h = 10$  (b). Other parameters correspond to those in Fig. Figure 2.

shows contour maps of the monomer density for different particle separations and particle heights  $h$  and compares them with the corresponding contour maps in good solvent. In poor solvent, the brush forms a dense layer with constant density, which is separated from the solvent by a well-defined interface located at  $h_b = 22 - 25$  (depending on  $h$ ; since the nanoparticles occupy volume, the brush layer thickens when the particles are inside). The behavior of the pair interactions can be correlated to their position with respect to the brush surface. As long as the particles are totally surrounded by brush polymers (at  $h = 10, 12$ ), the interaction is repulsive like in the swollen brush. When the nanoparticles touch the brush surface ( $h \geq 14$ ), the interaction vanishes almost entirely. As they are moved across the interface, an attractive contribution emerges, which has initially a rather short range (at  $h = 18$ ), but becomes longer ranged as  $h$  increases further. The attraction is maximal at  $h \approx 20$ , then it decreases and finally disappears once the nanoparticles have left the brush.

Based on these observations, we distinguish between an immersed regime ( $h = 10, 12$ ) where the nanoparticles are buried in the brush, and an interfacial regime ( $h \geq 14$ ) where the nanoparticles interact directly with the surface. The immersed regime can be characterized as follows: The nanoparticles are surrounded by melt-like polymer material. (For example, the polymer density increases much less in the gap between the nanoparticles than in the swollen brush, see Fig. Figure 3(b)). Nevertheless, the nanoparticles strongly perturb the larger-scale structure of the brush, especially in the region above them. The polymer density is depleted and the brush-solvent interface is pulled towards the nanoparticle. As two nanoparticles approach each other, their corresponding perturbed regions merge. As a result, the interaction energy  $U$  decreases (see Fig. Figure 2(f), curves for  $h = 10, 12$ ), indicating that the number of unfavorable polymer-solvent contacts decreases. This is however overcompensated by a substantial loss of solvent entropy, such that the solvent free energy increases. Since the polymer entropy also drops down (we will discuss this in Sec. Section 4), the total pair interaction is repulsive.

In the interfacial regime, the nanoparticles touch or cross the interface, and several phenomena influence the effective pair interaction.

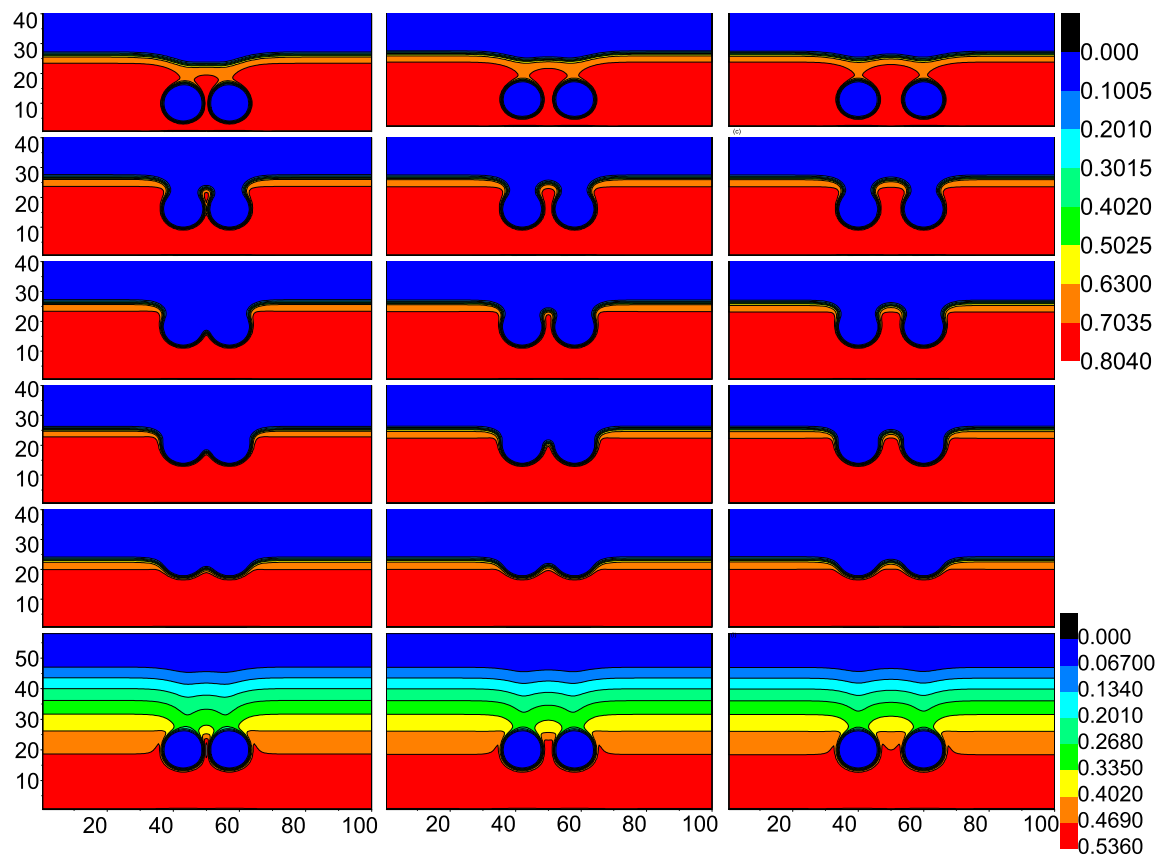


Fig. 4: Contour maps of polymer volume fraction profiles for the system studied in Fig. Figure 2 at particle separation  $d = 4$  (left),  $d = 6$  (middle), and  $d = 10$  (right), for poor solvent conditions and nanoparticle-substrate distance  $h = 10, 16, 18, 20, 24$  (first five rows), and for good solvent conditions and  $h = 20$  (last row).

- (i) The nanoparticles distort the polymer-solvent interface. Since the nanoparticle surface favors solvent over polymer for entropic reasons, the contact angle with respect to the polymer phase is higher than  $\pi/2$ . The interface bends around in order to meet the nanoparticle surface at the contact angle (see Fig. Figure 4). This leads to capillary interactions.<sup>60</sup> In addition, Fig. Figure 4 also suggests that the structure of the interface is perturbed in the vicinity of the nanoparticles, which may lead to additional interactions.
  
- (ii) If the particle height  $h$  is lower than the brush thickness  $h_b$ , the polymer-solvent interface can reduce its area in the gap between the particles by moving down, i.e. , by reducing its local position  $z_i$ . Even for  $h > h_b$ , it may still be beneficial to reduce  $z_i$  in order to better accommodate the contact angle. The resulting force on the interface is counteracted by the pressure of the brush. For  $h \leq 16$ , the interface in the gap stays at  $z_i = h_b$  at all particle separations (Fig. Figure 4, second panel). At  $h = 18$ , it jumps sharply between  $z_i = h_b \approx 22$  and  $z_i \approx h$  at particle separation  $d \sim 5$ . (Fig. Figure 4, third panel). At  $h \geq 20$ , it moves downwards continuously with decreasing  $d$ . The relocation of the interface is accompanied by a decrease of polymer-solvent contacts (see the corresponding curves for  $U$  in Fig. Figure 2).
  
- (iii) Due to the increased brush pressure, the relocated interface is narrower and has a higher interfacial energy than the interface outside of the particles. Hence the total free energy decreases if the gap between the particles becomes smaller, which results in an attractive interaction.

The interplay of these effects is responsible for the complex behavior of the pair interactions shown in Fig. Figure 2.

### 3.2 Influence of grafting density and particle size

Next we discuss the influence of grafting density and particle size on the effective pair interactions. Fig. Figure 5 shows the results for different grafting densities for particles of size  $R = 1.25R_g = 5.1$

at fixed height  $h = 16$  for good and poor solvent. The curves are very similar to Fig. Figure 2 (top panel). When the grafting density is increased, the brush thickness increases. Hence the distance between particles and the brush surface increases. This has the same effect than varying the height  $h$  at fixed grafting density.

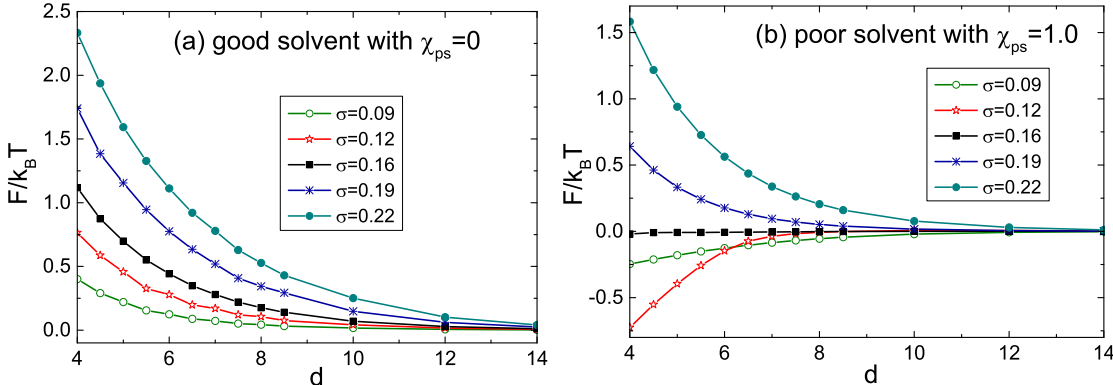


Fig. 5: Effective pair interactions in lateral directions of particles with size  $R = 1.25R_g = 5.1$  located at  $h = 16$  as a function of particle separation  $d$  in brushes with different grafting densities  $\sigma$  as indicated under good (a) and poor (b) solvent conditions.

Likewise, the effect of varying the particle size is investigated in Fig. Figure 6 (grafting density  $\sigma = 0.16$ , particle position  $h = 16$ ). Here, we find that increasing the particle size has the same effect as increasing the grafting density or decreasing  $h$  in Fig. Figure 2. The reason is that larger nanoparticles fill more space and expel monomers, which leads to a thickening of the brush in their vicinity. Therefore, at  $h = 16$ , large particles are still largely buried in the brush whereas small particles sit in the interface.

### 3.3 Effective interactions in vertical and diagonal directions

Finally, we briefly discuss the effective interactions for rod-like nanoparticles who's cross-sections are oriented vertically or diagonally with respect to the substrate. Fig. Figure 7 shows the effective interactions for three angles and compares them with the horizontal case. We find that vertically aligned nanoparticles always attract each other. The range of the attraction is given by the brush thickness. In good solvent, the range is therefore much larger than the range of the repulsive interaction in lateral direction. In poor solvent, the brush is thinner, and the range is comparable. The

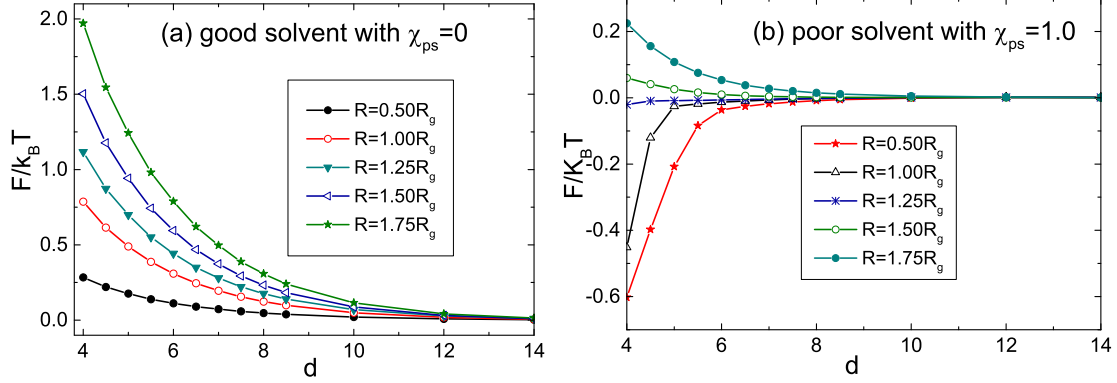


Fig. 6: Effective pair interactions in lateral directions of particles located at  $h = 16$  with different sizes  $R$  as indicated (ranging from  $R = 0.5R_g = 2$  to  $R = 1.75R_g = 7.1$ ) as a function of particle separation  $d$  in brushes under good (a) and poor (b) solvent conditions. The grafting density is  $\sigma = 0.16$ .

transition from vertical to lateral is not linear. In diagonal directions, repulsive barriers may appear both under good and poor solvent conditions, which separate a region of attractive interaction at short distances and a region of repulsive interaction at large distances.

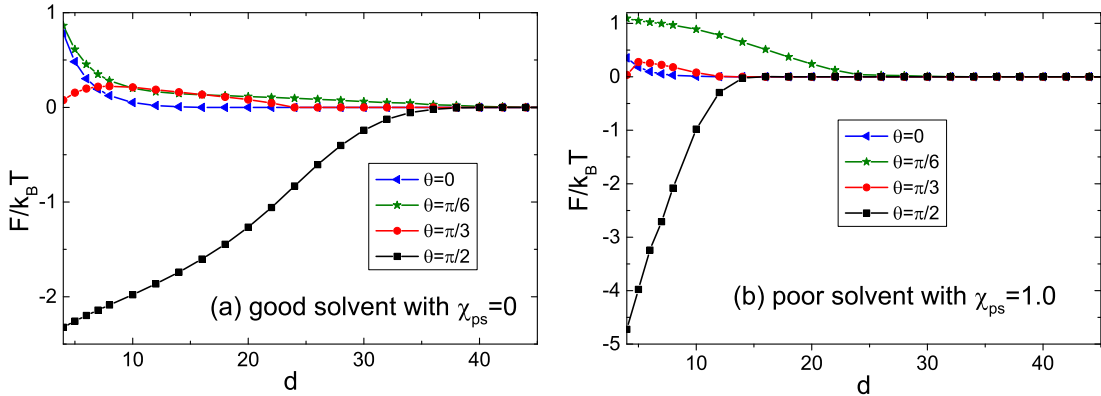


Fig. 7: Effective pair interactions of particle oriented with different angles  $\theta$  with respect to the substrate as a function of particle separation  $d$ , for brushes under good solvent conditions and  $h = 16$  (a), and for brushes under poor solvent conditions and  $h = 12$  (b). Here  $h$  is the distance between the substrate and the closest particle (see Fig. Figure 1). The particles have the size  $R = 0.75R_g = 3.1$  and the grafting density is  $\sigma = 0.16$ .

The corresponding density maps are shown in Fig. Figure 8. They suggest that the interactions are driven by the regions of lower polymer density that build up above the nanoparticles. If one particle is located in the polymer-depleted “wake” of another particle, they attract each other. Outside the depletion regions, the interaction between immersed particles tends to be repulsive.

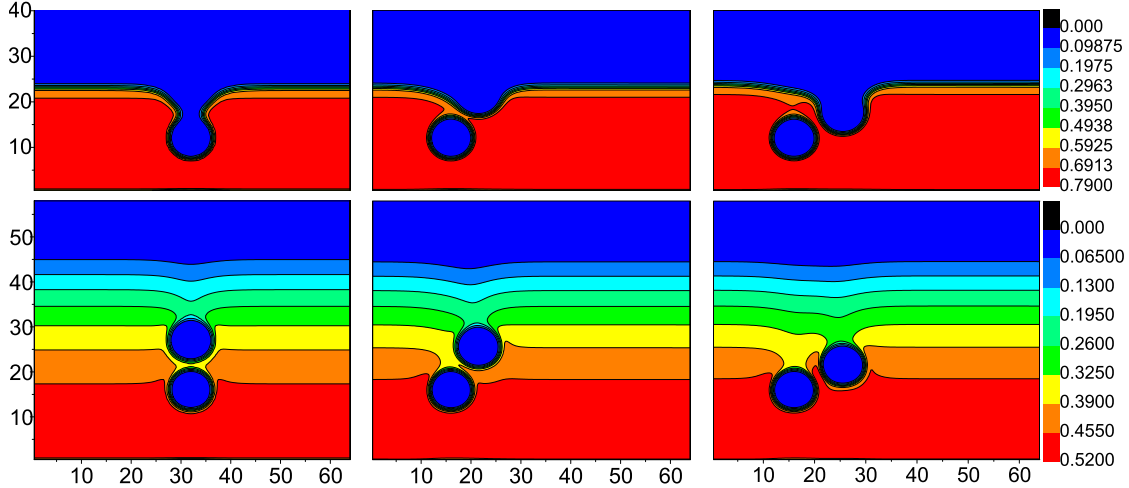


Fig. 8: Contour maps of polymer volume fraction profiles for the system studied in Fig. Figure 7 at particle separation  $d = 5$  and relative orientation  $\theta = \pi/2$  (left),  $\theta = \pi/3$  (middle), and  $\theta = \pi/6$  (right). Top panels show results for poor solvent and  $h = 12$ , bottom panels results for good solvent and  $h = 16$ .

## 4 Discussion and Summary

In the present paper, we have calculated the interactions between rod-like nanoparticles in polymer brushes under good and poor solvent conditions. In vertical directions ( $\theta = \pi/2$ ), the interactions are always attractive and act across the entire brush. In lateral direction ( $\theta = 0$ ), they depend on the solvent quality. For good solvent, they are repulsive. For poor solvent, we have identified two different regimes. If the nanoparticles are immersed in the brush, the interaction is repulsive. If they are located at the polymer-solvent interface, it is attractive.

We will now discuss our findings in the context of theoretical work in the literature, starting with the immersed regime for collapsed brushes (poor solvent) where the particles are fully surrounded by the brush and the monomer density inside the brush is roughly constant. This case was first discussed by Williams and Pincus<sup>23</sup> and later by a number of other authors.<sup>31,32,61</sup> Williams and Pincus used a strong stretching approximation,<sup>62</sup> where the statistical properties of each polymer are described in terms of a well-defined “mean path”  $\mathbf{R}_m(s)$ , and assumed that chains have infinite length, i.e. there are no chain ends inside the brush. They showed that the brush can then be mapped onto an Euler fluid: In the strong stretching limit, the free energy associated with

polymer stretching is written as

$$F = \sum_i \frac{3N}{2b^2} \int_0^1 ds \left( \frac{d\mathbf{R}_m(s)}{ds} \right)^2 = \frac{3N}{2b^2} \rho \int_{V_{\text{brush}}} dV \mathbf{v}(\mathbf{r})^2, \quad (14)$$

where  $\rho$  is the density inside the brush, the vector field  $\mathbf{v} = d\mathbf{R}_m(s)/ds$ , the sum  $\sum_i$  runs over all chains, the spatial integral on the right hand side runs over the volume inside the brush, and they have assumed incompressibility inside the brush. The free energy is minimized for rotation free vector fields  $\mathbf{v}$  that can be derived from a potential,  $\mathbf{v} = -\nabla\Phi$ , where  $\Delta\Phi = 0$  due to the incompressibility condition  $\nabla \cdot \mathbf{v} = 0$ . This is basically the Euler equation for potential flows. The only difference is that the local pressure enters the Bernoulli equation with opposite sign in the polymer brush,<sup>23</sup> i.e., it is given by  $p = \rho\mathbf{v}^2/2 + \text{const.}$  in the polymer brush system. Hence nanoparticles are driven towards regions of low “velocities”  $\mathbf{v}$ . This explains why they attract each other in the vertical direction (they are driven towards each others’ “wake”), and repel each other in the lateral direction.<sup>61</sup> Solis and Tang<sup>31</sup> have extended the theory to brushes of finite thickness, assuming that all chain ends are located at the brush surface (Alexander brush<sup>63</sup>). They predicted that the brush surface is pulled towards the nanoparticle, which is compatible with our findings in Fig. Figure 4 (top panel). In reality, chain ends are not pinned to the brush surface, but distributed in the whole brush.<sup>62,64,65</sup> Solis and Tang showed that this does not change the general picture.<sup>32</sup>

Hence the behavior of nanoparticles in the immersed regime seems to be well described by the hydrodynamic analogy. Interestingly, this holds even for swollen brushes, even though the theory was originally developed for dry brushes. However, as the nanoparticles enter the polymer-solvent interface, the picture breaks down and one enters the interfacial regime, a new regime which was not discussed in the previous studies. Here, the effective interactions are dominated by the effect of the nanoparticles on the interface, i.e., interfacial distortions and capillary interactions. These depend on the brush because the brush pressure generates a position dependent, inhomogeneous stress field in the interface. Apart from that, the direct interaction of the brush with the nanoparticles plays a minor role. Capillary interactions at fluid-fluid interfaces have been discussed intensely

in the colloid community.<sup>60</sup> However, to our best knowledge, this particular problem has not yet been studied.

We should note that another possible mechanism of attraction is polymer depletion. The depletion interaction was originally derived for dilute polymer solutions,<sup>3</sup> but since depletion layers may also be present in dense systems,<sup>6</sup> it could also be a possible source of interaction there. Indeed, it has presumably been observed in a self-consistent field study by Chen and Ma,<sup>33</sup> who considered nanoparticle interactions in a dense brush exposed to a polymer melt. For nanoparticles that are sufficiently far from the substrate, and for nanoparticles in pure melts (no brush), Chen and Ma reported a very short range attractive interaction. It only acts at very short distances, where the boundary layers of nanoparticles overlap. In our system, we have not observed this effect (data not shown) - presumably due to the fact that our nanoparticle surface is modeled in a slightly different manner.

In the present calculation, we have assumed that grafting points are mobile within the substrate. This is true for liquid substrates, but not valid for solid substrates and grafting by covalent bonds. However, we expect that the qualitative behavior will not be affected by the type of grafting. For nanoparticles close to the substrate, the additional constraint due to fixed grafting points<sup>66</sup> should further enhance the lateral repulsive forces<sup>67,68</sup>. If the nanoparticles are far from the substrate and/or within the interface the distribution of grafting points will not be affected by their presence in a significant manner.

In the present two-dimensional calculation, we have considered nanoparticles of infinitely long rod-like shape. Nevertheless, we believe that the physical interaction mechanisms discussed here – most notably the qualitative difference between interactions of nanoparticles that are immersed in the brush and those mediated by the brush-solvent interface – are generic and will remain valid for nanoparticles of arbitrary shape.

To summarize, we find that the lateral pair interactions between nanoparticles can change fundamentally as a function of solvent quality. The crucial difference between the swollen and the collapsed brush is that the collapsed brush has a well-defined narrow interface with the solvent,

with the characteristics of a fluid-fluid interface. Non-adsorbing nanoparticles like the ones studied here are expelled from the brush under both good and poor solvent conditions.<sup>30</sup> They could be driven into the brush, e.g., by long-range interactions with the substrate, by an external field, or by osmotic pressure. In such cases, they will penetrate the swollen brush to some extent. In collapsed brushes, however, they will likely be trapped at the polymer-solvent interface, since nanoparticles generally tend to have a preference for interfacial adsorption. Thus the lateral interactions in the swollen brush will be repulsive as characteristic for the immersed regime, and governed by interfacial interactions in the collapsed brush, implying that they are most likely attractive.<sup>60</sup> This opens the possibility to manipulate nanoparticle interactions by exchanging solvent. Another option is to use collapsed brushes throughout and tune the penetration depth of the nanoparticles with external fields. This also allows one to control the particle-particle interactions in a reversible manner by switching between the interfacial and the immersed regime. We hope that the present paper will motivate experiments in this direction.

## Acknowledgement

This work was supported by the National Natural Science Foundation of China (No.11304169), the Natural Science Foundation of Ningbo (No. 2012A110178) and the Science Foundation of Ningbo University (No.XK211202). It is sponsored by K.C.Wong Magna Fund in Ningbo University of China. J. Z. acknowledges support from the German Science Foundation (DFG) within SFB 1066, and S. Q. was supported from the DFG within SFB TRR 146. Computational resources at JGU Mainz (MOGON) are gratefully acknowledged.

## References

- [1] Winey, K. I.; Vaia, R. A. *MRS Bulletin* **2007**, *32*, 314–322.
- [2] Hosokawa, M., Nogi, K., Naito, M., Yokoyama, T., Eds. *Nanoparticle Technology Handbook*; Elsevier, 2012.

- [3] Asakura, S.; Oosawa, F. *J. Chem. Phys.* **1954**, *22*, 1255.
- [4] Asakura, S.; Oosawa, F. *J. Polym. Sci.* **1958**, *33*, 183–192.
- [5] Binder, K.; Virnau, P.; Statt, A. *J. Chem. Phys.* **2014**, *141*, 140901.
- [6] Fleer, G. J.; Skvortsov, A. M.; Tuinier, R. *Macromolecules* **2003**, *36*, 7857–7872.
- [7] Inoue, Y.; Nakanishi, T.; Ishihara, K. *Langmuir* **2013**, *29*, 10752–10758.
- [8] Sakata, S.; Inoue, Y.; Ishihara, K. *Langmuir* **2014**, *30*, 2745–2751.
- [9] Tan, K. Y.; Lin, H.; Ramstedt, M.; Watt, F. M.; Huck, W. T. S.; Gautrot, J. E. *Integr. Biol.* **2013**, *5*, 899–910.
- [10] Yang, W. J.; Neoh, K.-G.; Kang, E.-T.; Teo, S. L.-M.; Rittschof, D. *Prog. Polym. Sci.* **2014**, *39*, 1017–1042.
- [11] Kumar, S.; Tong, X.; Dory, Y. L.; Lepage, M.; Zhao, Y. *Chem. Commun.* **2013**, *49*, 90–92.
- [12] Huang, X.; Li, M.; Green, D. C.; Williams, D. S.; Patil, A. J.; Mann, S. *Nat. Commun.* **2013**, *4*, 2239.
- [13] Cappello, J.; Crissman, J.; Crissman, M.; Ferrari, F.; Textor, G.; Wallis, O.; Whitley, J.; Zhou, X.; Burman, D.; Aukerman, L.; Stedronsky, E. *J. Control. Release* **1998**, *53*, 105–117.
- [14] Abbott, D., N. L. an Blankschtein; Hatton, T. A. *Bioseparation* **1990**, *1*, 191–225.
- [15] Stano, A.; Scott, E. A.; Dane, K. Y.; Swartz, M. A.; Hubbell, J. A. *Biomaterials* **2013**, *34*, 4339–4346.
- [16] Cai, X.; Chen, J.; Xu, H.; Liu, S.; Jiang, Q.-X.; Halfmann, R.; Chen, Z. *J. Cell* **2014**, *156*, 1207–1222.
- [17] Feng, J.; Cavicchi, K. A.; Heinz, H. *ACS Nano* **2011**, *5*, 9413–9420.

- [18] Curk, T.; Martinez-Veracoechea, F. J.; Frenkel, D.; Dobnikar, J. *Nano Lett.* **2014**, *14*, 2617–2622.
- [19] de Groot, G. W.; Demarche, S.; Santonicola, M. G.; Tiefenauer, L.; Vancso, G. J. *Nanoscale* **2014**, *6*, 2228–2237.
- [20] Poelma, J. E.; Fors, B. P.; Meyers, G. F.; Kramer, J. W.; Hawker, C. J. *Angewandte Chemie* **2013**, *125*, 6982–6986.
- [21] Park, S. H.; Lee, H. S.; Kim, J.-D.; Breiby, D. W.; Kim, E.; Park, Y. D.; Ryu, D. Y.; Lee, D. R.; Cho, J. H. *J. Mater. Chem.* **2011**, *21*, 15580–15586.
- [22] Lin, X.; He, Q.; Li, J. *Chem. Soc. Rev.* **2012**, *41*, 3584–3593.
- [23] Williams, D. R. M.; Pincus, P. A. *Europhys. Lett.* **1993**, *24*, 29–34.
- [24] Subramanian, G.; Williams, D. R. M.; Pincus, P. A. *Macromolecules* **1996**, *29*, 4045–4050.
- [25] Steels, B. M.; Leermakers, F. A. M.; Haynes, C. A. *J. Chromatogr. B* **2000**, *743*, 31–40.
- [26] Satulovsky, J.; Carignano, M. A.; Szleifer, I. *Proc. Natl. Acad. Sci.* **2000**, *97*, 9037–9041.
- [27] Currie, E.; Norde, W.; Cohen Stuart, M. A. *Adv. Colloid Interfac. Sci.* **2003**, *100*, 205–265.
- [28] Kim, J. U.; O’Shaughnessy, B. *Phys. Rev. Lett.* **2002**, *89*, 238301.
- [29] Qi, S.; Behringer, H.; Schmid, F. *New J. Phys.* **2013**, *15*, 125009.
- [30] Halperin, A.; Kroger, M.; Zhulina, E. B. *Macromolecules* **2011**, *44*, 3622–3638.
- [31] Solis, F. J.; Tang, H. *Macromolecules* **1996**, *29*, 4060–4065.
- [32] Solis, F. J.; Tang, H. *Macromolecules* **1996**, *29*, 7953–7959.
- [33] Chen, K.; Ma, Y.-q. *J. Phys. Chem. B* **2005**, *109*, 17617–17622.

- [34] Curk, T.; Martinez-Veracoechea, F. J.; Frenkel, D.; Dobnikar, J. *Soft Matter* **2013**, *9*, 5565–5571.
- [35] Guskova, O. A.; Pal, S.; Seidel, C. *Europhys. Lett.* **2009**, *88*, 38006.
- [36] Guskova, O. A.; Seidel, C. *Soft Matter* **2012**, *8*, 2833–2843.
- [37] Cole, M. A.; Voelcker, N. H.; Thissen, H.; Griesser, H. J. *Biomaterials* **2009**, *30*, 1827–1850.
- [38] Yang, J.; Yamato, M.; Okano, T. *MRS Bulletin* **2005**, *30*, 189–193.
- [39] da Silva, R. M.; Mano, J. F.; Reis, R. L. *Trends Biotechnol.* **2007**, *25*, 577–583.
- [40] Chiu, J. J.; Kim, B. J.; Yi, G.-R.; Bang, J.; Kramer, E. J.; Pine, D. J. *Macromolecules* **2007**, *40*, 3361–3365.
- [41] Murat, M.; Grest, G. S. *Macromolecules* **1989**, *22*, 4054–4059.
- [42] Milner, S. T.; Witten, T. A.; Cates, M. E. *Macromolecules* **1988**, *21*, 2610–2619.
- [43] Espinosa-Marzal, R. M.; Nalam, P. C.; Bolisetty, S.; Spencer, N. D. *Soft Matter* **2013**, *9*, 4045–4057.
- [44] Cohen Stuart, M. A.; Huck, W. T. S.; Genzer, J.; Müller, M.; Ober, C.; Stamm, M.; Sukhorukov, G. B.; Igal Szleifer, V. V. T.; Urban, M.; Winnik, F.; Zauscher, S.; Luzinov, I.; Minko, S. *Nat. Mater.* **2010**, *9*, 101–113.
- [45] Klushin, L. I.; Skvortsov, A. M.; Polotsky, A. A.; Qi, S.; Schmid, F. *Phys. Rev. Lett.* **2014**, *113*, 068303.
- [46] Schmid, F. *J. Phys.: Condens. Matter* **1998**, *10*, 8105.
- [47] Matsen, M. In *Soft Matter, Volume 1: Polymer Melts and Mixtures*; Gompper, G., Schick, M., Eds.; Wiley-VCH: Weinheim, 2006.

- [48] Fredrickson, G. H. *The Equilibrium Theory of Inhomogeneous Polymers*; Clarendon Press: Oxford, 2006.
- [49] Naughton, J. R.; Matsen, M. W. *Macromolecules* **2002**, *35*, 5688–5696.
- [50] Pryamitsyn, V.; Ganesan, V. *J. Chem. Phys.* **2013**, *138*, 234905.
- [51] Pryamitsyn, V.; Ganesan, V. *Macromolecules* **2014**, *47*, 6095–6112.
- [52] Thompson, R.; Ginzburg, V.; Matsen, M.; Balazs, A. *Science* **2001**, *292*, 2469–2472.
- [53] Lee, J. Y.; Shou, Z.; Balazs, A. C. *Phys. Rev. Lett.* **2003**, *91*, 136103.
- [54] Sides, S. W.; Kim, B. J.; Kramer, E. J.; Fredrickson, G. H. *Phys. Rev. Lett.* **2006**, *96*, 250601.
- [55] Matsen, M. W. *J. Chem. Phys.* **1997**, *106*, 7781.
- [56] Flory, P. J. *J. Chem. Phys.* **1949**, *17*, 303–310.
- [57] Helfand, E. *J. Chem. Phys.* **1975**, *62*, 999–1005.
- [58] Hong, K. M.; Noolandi, J. *Macromolecules* **1981**, *14*, 727–736.
- [59] de Gennes, P. G. *Scaling Concepts in Polymer Physics*; Cornell University Press, 1979.
- [60] Bresme, F.; Oettel, M. *J. Phys.: Cond. Matter* **2007**, *19*, 413101.
- [61] Kim, J. U.; O’Shaughnessy, B. *Macromolecules* **2006**, *39*, 413–425.
- [62] Semenov, A. N. *Sov. Phys. JETP* **1985**, *61*, 733–742.
- [63] Alexander, S. *J. Phys. (Paris)* **1977**, *38*, 983–987.
- [64] Milner, S. T.; Witten, T. A.; Cates, M. E. *Macromolecules* **1988**, *21*, 2610–2619.
- [65] Zhulina, E.; Borisov, O.; Priamitsyn, V. *J. Colloid Interface Sci.* **1990**, *137*, 495–511.
- [66] Müller, M. *Physical Review E* **2002**, *65*, 030802.

[67] Kim, J. U.; Matsen, M. W. *Macromolecules* **2008**, *41*, 246–252.

[68] Kim, J. U.; Matsen, M. W. *Macromolecules* **2008**, *41*, 4435–4443.

# Graphical TOC Entry

